Nonmonotonic traveling wave solutions of infiltration into porous media

David A. DiCarlo,[1] Ruben Juanes,[2] Tara LaForce,[3] and Thomas P. Witelski[4]

Received 15 February 2007; revised 27 July 2007; accepted 12 October 2007; published 5 February 2008.

[1] In uniform soils that are susceptible to unstable preferential flow, the water saturation may exhibit a nonmonotonic profile upon continuous infiltration. As this nonmonotonicity (also known as saturation overshoot) cannot be described by the conventional Richards equation, there have been proposed possible extensions to the unsaturated flow equations, including a nonmonotonic capillary pressure–saturation curve and a second-order hyperbolic term. Here, we present analytic traveling wave solutions to the extended Richards equation. These new solutions indeed display a nonmonotonic saturation profile, similar to previous simulation results. We show that these extensions need a regularization term to produce a unique solution. We develop complete analytic solutions using a relaxation regularization term, and we discuss the results in terms of recent measurements of saturation overshoot.

Citation: DiCarlo, D. A., R. Juanes, T. LaForce, and T. P. Witelski (2008), Nonmonotonic traveling wave solutions of infiltration into porous media, *Water Resour. Res.*, *44*, W02406, doi:10.1029/2007WR005975.

1. Introduction

[2] Experiments have shown that constant flux infiltrations into laterally confined, sandy porous media will result in the saturation (and water pressure) being higher at the initial wetting front than behind the front for a wide range of applied fluxes. This has been dubbed saturation overshoot, as the saturation overshoots its asymptotic value, with the resultant nonmonotonic saturation and pressure profiles [*Stonestrom and Akstin*, 1994; *Geiger and Durnford*, 2000; *DiCarlo*, 2004; *Shiozawa and Fujimaki*, 2004]. Experimental measurements of overshoot are shown in Figure 1. This is for a constant infiltration of 0.8 cm/min into a 20/30 (median diam of 0.71 mm) sand. Both the saturation profile (measured using light transmission) and the pressure profile (measured with a tensiometer) clearly do not move monotonically from their initial values to their final values, but instead "overshoot" these values at the initial front before moving slowly to their asymptotic values. The importance of saturation overshoot manifests itself in two forms: first, saturation overshoot has been hypothesized to be the cause of gravity driven fingering [*Geiger and Durnford*, 2000; *Eliassi and Glass*, 2001; *Egorov et al.*, 2003], and second, saturation overshoot cannot be modeled by standard descriptions of unsaturated flow [*Eliassi and Glass*, 2001, 2002; *Egorov et al.*, 2003; *DiCarlo*, 2005]. Here we concentrate on the latter.

[3] Unsaturated flow in porous media is typically modeled by the Richards equation. This equation, which describes the evolution of water saturation in an unsaturated porous medium, is simply a combination of conservation of mass, the Darcy-Buckingham unsaturated flux equation, and the soil characteristic pressure–saturation curve [*Hillel*, 1980; *Dullien*, 1992], and is expressed in one spatial dimension as

$$\phi \frac{\partial S}{\partial t} - \frac{\partial}{\partial z}\left[K(S)\left(\frac{\partial P_w}{\partial z} - 1\right)\right] = 0. \tag{1}$$

[4] Here z is positive downward, ϕ is the porosity, S is the water saturation (water content as a fraction of pore space), $K(S)$ is the unsaturated conductivity, and P_w is the water pressure in units of head. Implicit in the Richards equation is the assumption that one can define a length scale where properties such as porosity, conductivity, and saturation can be considered continuous [*Bear*, 1972].

[5] This second-order partial differential equation (PDE) cannot produce the observed nonmonotonic profiles for constant boundary conditions and monotonic P-S and K-S curves due to its diffusive nature [*Eliassi and Glass*, 2001; *Egorov et al.*, 2003; *Nieber et al.*, 2005]. Because of this *Eliassi and Glass* [2002] proposed three different possible continuum extensions that cause water to be held back at the wetting front. They called these terms respectively, a hypodiffusive term (second order in space), a hyperbolic term (second order in time), and mixed or relaxation term (second order in space, first order in time). Using the hypodiffusive term, they were able to produce nonmonotonic profiles in numerical simulations [*Eliassi and Glass*, 2003].

[6] Most studies have concentrated on the relaxation term extension. *Cuesta et al.* [2000] analyzed a mathematical model of infiltration with a relaxation term, establishing existence of traveling wave solutions which exhibit oscilla-

[1] Petroleum and Geosystems Engineering, The University of Texas at Austin, Austin, Texas, USA.
[2] Department of Civil and Environmental Engineering, Massachusetts Institute of Technology, Cambridge, Massachusetts, USA.
[3] Department of Earth Science and Engineering, Imperial College London, London, UK.
[4] Department of Mathematics, Duke University, Durham, North Carolina, USA.

0043-1397/08/2007WR005975$09.00

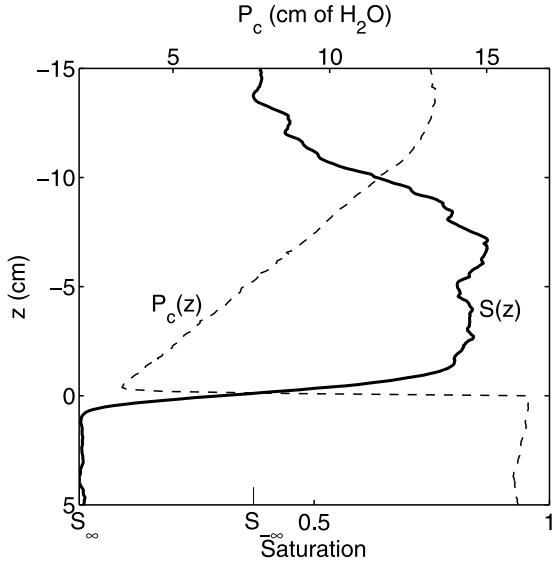

Figure 1. Measured saturation (solid line) and pressure profile (dashed line) for a constant infiltration of 0.8 cm/min into 20/30 sand.

tory (nonmonotonic) behavior if the effect of dynamic capillary pressure is sufficiently large. *Cuesta and Hulshof* [2003] studied a related system in which the original Richards equation simplifies to the Burgers equation, and the relaxation term is assumed to be linear. *Van Duijn et al.* [2007] studied the related problem of the Buckley-Leverett equation, which describes flow of two fluids through porous media, when the mobilities of both fluids are finite–in the Richards equation, air is assumed to be infinitely mobile. They found new, nonmonotonic solutions, when a third-order relaxation term is included. Their study is limited to the case of vanishing capillarity and relaxation. *Nieber et al.* [2005] gave a review of mathematical analyses of the Richards equation with static and dynamic capillary pressure–saturation relationships. In addition to a thorough stability analysis of the equations, nonmonotonic analytical solutions were found when a relaxation term (due to dynamic capillary pressure) was included. *DiCarlo* [2005] used the relaxation term to achieve an analytic nonmonotonic solution by using the traveling wave properties of the observed infiltrations. The solutions were only nonmonotonic when the applied flux is above a critical flux, which depended on the magnitude of the additional term and the media properties.

[7] All of these studies employ a model with standard (monotonic) capillary pressure–saturation relationship, which leads to nonmonotonic traveling wave solutions when dynamic capillary pressure effects are sufficiently large. In contrast, in this paper, we present analytic traveling wave solutions when either the hypodiffusive or hyperbolic terms are included. We show that the inclusion of the hypodiffusive term of magnitude large enough to create overshoot produces nonunique solutions. The need for regularization in the case of dominating hypodiffusive terms can be explained by the fact that the non-regularized problem is similar to an inverse heat equation, which is not well posed. Uniqueness can be recovered by introducing an additional high-order term (also known as a regularization term), and letting the magnitude of this regularization term go to zero. We employ the dynamic capillary pressure concept to introduce such (vanishing, as opposed to large) regularization term. Using the same analysis, we show how to construct solutions when the hyperbolic (second-order in time) term is included. In both cases, the solutions are sensitive to the form of the regularization term even in the limit of vanishing regularization. Our analysis illustrates the fine balance between capillarity and relaxation effects required to guarantee uniqueness of the solution. We finally discuss the two solutions in context of experimental measurements of saturation overshoot.

2. Problem Background

[8] Traditionally, the water content in the unsaturated zone has been modeled using Richards equation (equation (1)). If we assume the air pressure (P_a) is constant, the water pressure is given by the negative capillary pressure (P_c):

$$P_c(S) = P_a - P_w. \tag{2}$$

[9] Here we take the traditional representation of the capillary pressure where the capillary pressure is dependent on the water saturation, and not the rate of change of the water saturation. This saturation dependence displays well known hysteresis [*Dullien*, 1992], with different curves for increasing (imbibition) or decreasing (drainage) water saturation. In either case, the capillary pressure invariably decreases monotonically with increasing water saturation for either imbibition or drainage. Combining equations (1) and (2), we get a PDE that describes the water saturation change with time:

$$\phi\frac{\partial S}{\partial t} + \frac{\partial}{\partial z}\left[K(S) + K(S)P_c'(S)\frac{\partial S}{\partial z}\right] = 0. \tag{3}$$

where

$$P_c'(S) = \frac{dP_c}{dS} \tag{4}$$

and is always negative for a monotonically decreasing capillary pressure. Equation (3) is a nonlinear conservation law of advection–diffusion type, where $K(S)$ is a convex function that plays the role of a (nonlinear) advective flux. It is useful to define the diffusivity

$$D(S) = -K(S)P_c'(S), \tag{5}$$

which plays the role of a (nonlinear) diffusion coefficient. It will be seen that nonmonotonic solutions occur if there is a region of negative diffusivity.

3. Traveling Wave Solution

[10] Infiltrations into porous media that exhibit saturation overshoot are observed to be traveling waves [*Selker et al.*, 1992; *DiCarlo*, 2004]. Thus we seek a traveling wave solution to equation (3). Writing $S(z, t)$ as $S(z - vt)$ gives a solution propagating downward at a velocity of v. Intro-

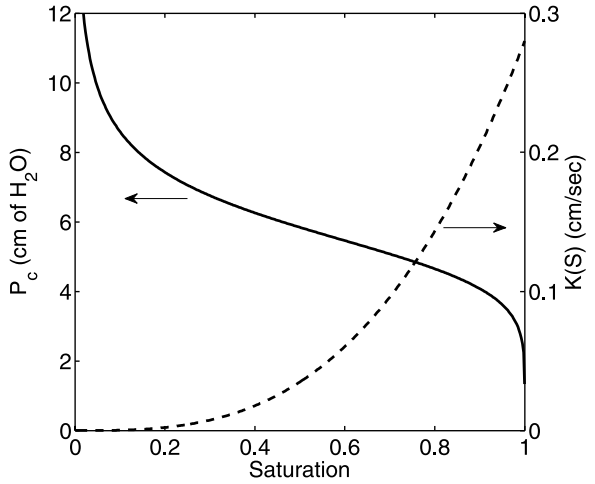

Figure 2. Imbibition capillary pressure curve (solid line) and unsaturated conductivity curve (dashed line) as functions of saturation. These curves are representative of 20/30 sand that produce nonmonotonic saturation profiles on infiltration.

ducing the new variable $\eta = z - vt$, the partial differentials become ordinary derivatives, and the PDE collapses to an ordinary differential equation (ODE):

$$-v\phi\frac{dS}{d\eta}+\frac{d}{d\eta}K(S)+\frac{d}{d\eta}\left[K(S)P_c'(S)\frac{dS}{d\eta}\right]=0. \tag{6}$$

[11] The equation above can be integrated imposing the following behavior at infinity:

$$\begin{aligned}\eta\to\infty &: S\to S_\infty, S'\to 0\\ \eta\to-\infty &: S\to S_{-\infty}, S'\to 0,\end{aligned} \tag{7}$$

to yield the following first-order ODE:

$$K(S)-K(S_\infty)-v\phi(S-S_\infty)+K(S)P_c'(S)\frac{dS}{d\eta}=0, \tag{8}$$

with the wave velocity given by the Rankine–Hugoniot condition

$$v=\frac{K(S_{-\infty})-K(S_\infty)}{\phi(S_{-\infty}-S_\infty)}. \tag{9}$$

[12] Given that the function $K(S)$ is convex, traveling wave solutions satisfying equations (8) and (9) can only exist if $S_{-\infty} > S_\infty$. This is indeed the case, as we are interested in solutions to infiltration, not drainage. Equation (8) can be solved by separation of variables and simple integration:

$$\eta(S)=\int_{S_\infty}^{S}\frac{-K(s)P_c'(s)}{K(s)-K(S_\infty)-v\phi(s-S_\infty)}ds. \tag{10}$$

[13] The traveling wave profile $\eta(S)$ is monotonic, as long as the unsaturated conductivity is positive and convex (increasing faster than linearly with saturation), and the capillary pressure is monotonically decreasing (i.e., the derivative of P_c is always negative). Hysteresis does not play a role in the solution as the saturation is monotonically increasing and the soil remains on the wetting curve. In Figure 2 we show representative capillary pressure and unsaturated conductivity curves. The functional forms and parameter values are given in Table 1. The solution to equation (10) using these functions is shown in Figure 3. The solution displays a sharp wetting front. We must remark, however, that the slope is not infinity in our case–it would have been if the initial conditions corresponded to a dry medium due to the vanishing diffusivity at $S = 0$.

Table 1. Functional Forms for the Constitutive Equations That are Used to Obtain the Solutions[a]

Name	Symbol	Functional Form
Unsaturated conductivity	$K(S)$	$K_s S^3$
Capillary pressure	$P_c(S)$	$\frac{1}{\alpha}(S_e^{(n/n-1)}-1)^{1/n}$
Nonmonotonic capillary pressure	$P_{cm}(S)$	$P_c(S) - N_{HD}\,\Lambda(S)$
Reduced saturation	S_e	$\frac{S-S_r}{1-S_r}$
Hypo-diffusive term	$\Lambda(S)$	$60S_e(.333S_e^2 - .503S_e + .187)$
Hyperbolic term	$\Gamma(S)$	$\Gamma = \Gamma' S$
Initial saturation	$S_{+\infty}$	0.0075
Final saturation (Figures 3, 5–7)	$S_{-\infty}$	0.95
Final saturation (Figures 8, 9, 11)	$S_{-\infty}$	0.57

[a]The soil parameters were taken from the 20/30 sand.

[14] Although the traveling wave solution to Richards equation cannot produce overshoot with standard constitutive curves (as seen in Figure 2), when overshoot does occur, the traveling wave solution accurately represents the

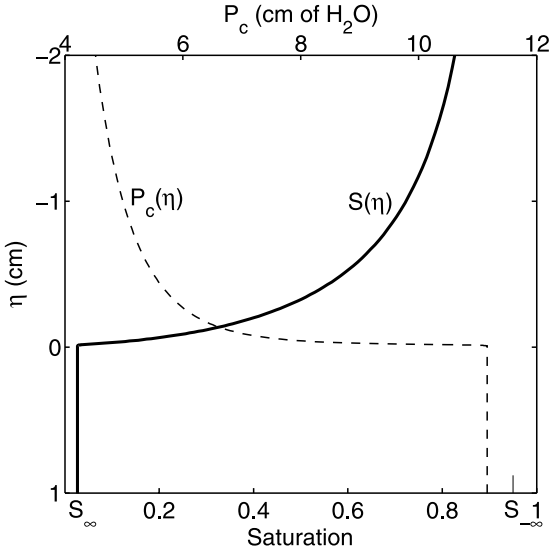

Figure 3. Saturation (solid line) and capillary pressure (dashed line) versus space obtained using the traveling wave solution and the constitutive curves in Figure 2 and Table 1.

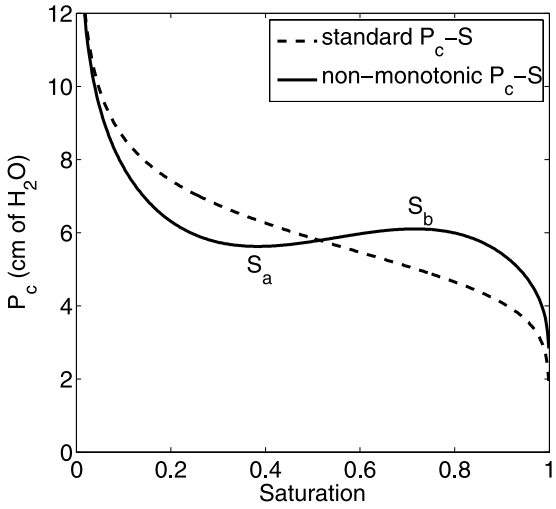

Figure 4. Standard imbibition capillary pressure curve for sand that exhibits saturation overshoot (dashed line). Proposed nonmonotonic imbibition capillary pressure curve (solid line).

drainage portion of the profile if the overshoot saturation is taken as the initial condition [*Selker et al.*, 1992].

4. Nonmonotonic Capillary Pressure Curve

[15] *Eliassi and Glass* [2002] proposed possible continuum extensions to the flux equation that would effectively discourage the initial wetting front from entering the dry media. In theory, this backs up the water and produces saturation profiles that are nonmonotonic. We first concentrate on the hypodiffusive (second order in space) term, which was used to numerically produce infiltrations that had nonmonotonic profiles [*Eliassi and Glass*, 2003]. They proposed to add the following term to the left hand side of Richards equation (equation (3)):

$$R_{hypo} = -\frac{\partial}{\partial z}\left[K(S)N_{HD}\frac{d\Lambda(S)}{dS}\frac{\partial S}{\partial z}\right], \tag{11}$$

where N_{HD} gives the magnitude of the hypo-diffusive term, and $\Lambda(S)$ is postulated to be a function of the saturation. They postulate that this term is the result of phase interfaces that influence the Helmholtz free energy based on the papers of Gray and Hassanizadeh [*Hassanizadeh and Gray*, 1990; *Gray and Hassanizadeh*, 1991]. *Eliassi and Glass* [2003] used the hypodiffusive term to produce saturation patterns which qualitatively matched up with those seen in gravity driven fingers. Including the hypodiffusive term gives the following extended Richards equation:

$$\phi\frac{\partial S}{\partial t} + \frac{\partial}{\partial z}\left[K(S) + K(S)\frac{dP_c(S)}{dS}\frac{\partial S}{\partial z}\right] - \frac{\partial}{\partial z}\left[K(S)N_{HD}\frac{d\Lambda(S)}{dS}\frac{\partial S}{\partial z}\right] = 0. \tag{12}$$

[16] From equation (12), it can be easily seen that the addition of the hypo-diffusive term can be completely absorbed into the capillary pressure term [*Eliassi and Glass*, 2003]. This incorporation results in the standard Richards equation with a "modified capillary potential"

$$P_{cm}(S) = P_c(S) - N_{HD}\Lambda(S). \tag{13}$$

[17] This incorporation makes physical sense as the hypodiffusive term is a term that moves water from higher energy to lower energy. As the capillary pressure already subsumes the forces that move unsaturated water in porous media (e.g., van der Waals energy, hydration energy, double layer energy, capillary energy, etc.), it is natural for the hypodiffusive term to be subsumed into the capillary pressure also.

[18] With this incorporation, overshoot solutions are found numerically, if and only if, the modified capillary pressure is nonmonotonic with respect to saturation [*Eliassi and Glass*, 2003]. Whether or not a nonmonotonic P_{cm}-S curve is physical is an open question, but we proceed with the aim of obtaining a traveling wave solution to Richards equation with a nonmonotonic P_{cm}-S curve on imbibition. Hence we will refer to the modified capillary pressure as the nonmonotonic capillary pressure, and will use the notation as P_{cm} for clarity throughout the rest of the paper.

[19] Figure 4 shows a nonmonotonic P_{cm}-S curve as well as a typical monotonic P_c-S curve. The monotonic P_c-S curve shown is a fit using a van Genuchten P_c-S curve to capillary rise experiments in 20/30 sand (0.71 mm), a sand that exhibits saturation overshoot for a range of fluxes. This particular P_{cm}-S curve is slightly different from the one postulated by *Eliassi and Glass* [2003], with a smaller smoother region of nonmonotonicity, and its functional form was chosen to illustrate the details in the solution. The arguments that follow work the same for any nonmonotonic P_{cm}-S curve. In Figure 4, the turning points (where the slope changes sign) in the P_{cm}-S curve are at S_a and S_b (with $S_a < S_b$), between which P_{cm} is increasing with increasing saturation.

[20] Following *Witelski* [1995, 1996], we first consider the case where the initial and final conditions are outside of the increasing P_{cm} interval. In particular, we shall assume that $S_\infty < S_a$ and $S_{-\infty} > S_b$, corresponding to a water infiltration process. The manipulations to obtain the traveling wave solution to the Richards equation presented above are still valid for a nonmonotonic capillary pressure, and thus we begin with equation (8), only replacing $P_c'(S)$ by $P_{cm}'(S)$.

[21] The integration of equation (8) with the nonmonotonic P_{cm}-S curve from Figure 4 and Tables 1 and 2 is shown in Figure 5. Because the sign of $P'_{cm}(S)$ changes in the region $S_a < S < S_b$, the solution is multivalued in space and hence cannot correspond to a physical solution of equation (8). The nonmonotonic behavior of the solution $\eta(S)$ is due to the fact that the diffusivity $D(S)$ is negative in the range $S_a < S < S_b$, resulting in a kind of forward-backward heat equation.

[22] In the spirit of weak (discontinuous) solutions to conservation laws, one may be tempted to replace the nonmonotonic region by a shock or discontinuity. However, while the saturation may be discontinuous in space, there is a requirement of pressure continuity as pressure gradients

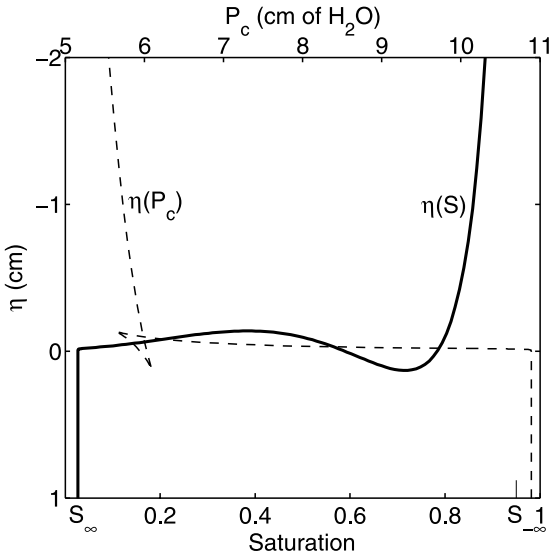

Figure 5. Solution to the saturation and capillary pressure profile on infiltration using equation (12) and the nonmonotonic capillary pressure curve in Figure 4. The solution is multivalued in space, which needs to be corrected by a shock.

drive the water flow and the Richards equation is first-order in time. Thus the upstream (S_-) and downstream (S_+) limiting values at the shock must satisfy

$$P_{cm}(S_-) = P_{cm}(S_+). \tag{14}$$

[23] From the structure of the solution (see Figure 5), it is clear that it is not possible to introduce a shock without creating a discontinuity in the capillary pressure. Moreover, both S_- and S_+ also must be outside the unstable interval of increasing capillary pressure, so that away from the shock the solution obtained by integrating equation (8) is not multivalued in space and thus is valid. All of the requirements above are satisfied by inserting a shock (a discontinuity traveling with speed v) at $\hat{\eta}_s$ (the shock position), and noting that traveling wave solutions can be arbitrarily translated with respect to η. The outer solution is then the two traveling wave solutions which exist over the positive diffusivity region, pasted together with a shock over the negative diffusivity region. This is written mathematically as (*Witelski*, 1996):

$$\hat{\eta}(S) = \hat{\eta}_s + \begin{cases} \eta(S) - \eta(S_-) \ \textit{for} \ \ \hat{\eta} < \hat{\eta}_s \\ \eta(S) - \eta(S_+) \ \textit{for} \ \ \hat{\eta} > \hat{\eta}_s \end{cases}. \tag{15}$$

[24] The question now is how to determine the values of S_- and S_+. Equation (15) is a one-parameter family of solutions in the sense that for each S_- there is a single S_+ that will satisfy equation (14). This type of problem has been studied before [*Hollig*, 1983], and it has been shown that in the absence of additional criteria all pairs are equally valid or, in other words, the solution is nonunique.

[25] The problem will have a unique solution if the influence of other higher order physical effects is incorporated. Mathematically, these additional terms are called regularization terms as they will determine the internal structure of the shock (equation (15)), but otherwise do not significantly influence the outer solution. Thus the regularization can be neglected in calculating the solution profile away from the shock.

[26] In what follows, we use the relaxation term arising from the dynamic capillary pressure concept as our higher order regularization term, although other regularization terms, such as a fourth-order in space regularization, are possible [*Witelski*, 1996]. The relaxation term has been advocated by Hassanizadeh and Gray [*Hassanizadeh and Gray*, 1990; *Hassanizadeh et al.*, 2002; *Egorov et al.*, 2003]. They postulate that the dynamic (actual) capillary pressure is related to the static capillary pressure through

$$P_{cd}(S) = P_{cm}(S) - \varepsilon\tau(S)\frac{\partial S}{\partial t}, \tag{16}$$

where $P_{cm}(S)$ is the static capillary pressure (i.e., the nonmonotonic capillary pressure we are using), $\tau(S)$ is a positive function modeling the water saturation-dependent relaxation term, and ε is a parameter that reflects the magnitude of the regularization. In what follows, we determine the unique solution to the problem *in the limit* $\varepsilon \to 0$ by using singular perturbation analysis [*Witelski*, 1996].

[27] With this additional dynamic capillary pressure term, the extended Richards equation reads:

$$\phi\frac{\partial S}{\partial t} + \frac{\partial}{\partial z}\left[K(S) + K(S)\frac{dP_{cm}(S)}{dS}\frac{\partial S}{\partial z}\right] - \varepsilon\frac{\partial}{\partial z}\left[K(S)\frac{\partial}{\partial z}\left(\tau(S)\frac{\partial S}{\partial t}\right)\right] = 0. \tag{17}$$

[28] We emphasize that in equation (17), P_{cm} is the static nonmonotonic capillary pressure, and the dynamic term will be taken to zero. Looking for a traveling wave solution of the form $S(z, t) = S(\eta)$ with $\eta = z - vt$, and integrating using the same behavior at infinity as before (equation (7)), we obtain the following ODE:

$$K(S) - K(S_\infty) - v\phi(S - S_\infty) + K(S)\frac{dP_{cm}(S)}{d\eta} + \varepsilon vK(S)\frac{d}{d\eta}\left(\tau(S)\frac{dS}{d\eta}\right) = 0. \tag{18}$$

[29] The fixed points of the solution are still S_∞ and $S_{-\infty}$, and the outer solution (in the limit $\varepsilon \to 0$) is still given by equations (8) and (15).

Table 2. Physical Parameters for the Three Sands[a]

Sand	d_{50} mm	K cm/min	ϕ	S_r	α cm^{-1}	n	S_p
12/20	1.105	30	0.35	0.001	0.303	5	0.25
20/30	0.713	15	0.35	0.001	0.178	6.3	0.25
30/40	0.532	9.0	0.35	0.001	0.15	10	0.4
20/30 drainage	0.713	15	0.35	0.001	0.10	10	0.25

[a]The van Genuchten parameters are for the imbibition curves, except for the bottom row where they are for the 20/30 drainage curve.

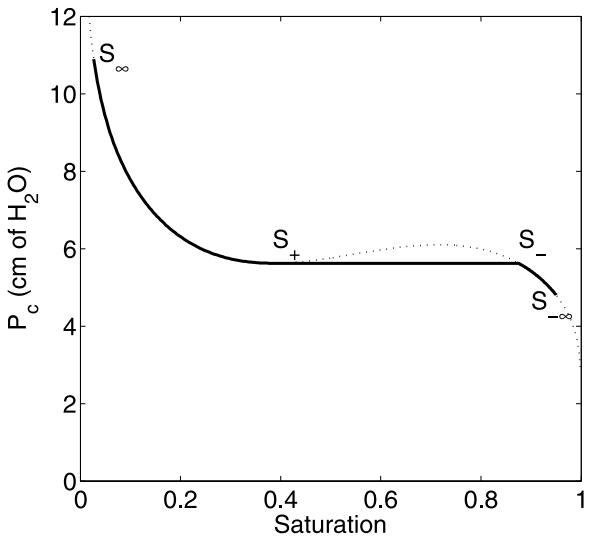

Figure 6. Construction of the shock endpoint saturations from the capillary pressure curve (solid line). The take off point (S_+) is at the local minimum of the capillary pressure curve (dotted line), and the landing point (S_-) is at equal capillary pressure.

[30] With the outer solution given by equations (8) and (15), the regularization term allows us to determine S_- and S_+ by resolving the inner structure of the shock. We follow *Witelski* [1996] and use singular perturbation analysis to resolve the structure of the shock in the limit $\varepsilon \to 0$ by introducing the stretched variable

$$\xi = \frac{\hat{\eta} - \hat{\eta}_s}{\varepsilon}, \tag{19}$$

where $\hat{\eta}_s$ is the shock position. Since ε is a small parameter, this stretching zooms into the structure of the solution around the shock. Equation (18) then reads

$$\varepsilon(K(S) - K(S_\infty) - v\phi(S - S_\infty)) + K(S)\frac{dP_{cm}(S)}{d\xi} + vK(S)\frac{d}{d\xi}\left(\tau(S)\frac{dS}{d\xi}\right) = 0. \tag{20}$$

[31] Integrating with respect to ξ, and to leading order, we obtain the desired balance between capillarity and the relaxation effect,

$$P_{cm}(S) + v\tau(S)\frac{dS}{d\xi} = B + O(\varepsilon), \tag{21}$$

where B is an integration constant. The behavior at infinity for equation (21) is

$$\begin{aligned} &\xi \to \infty : S \to S_+, S' \to 0 \\ &\xi \to -\infty : S \to S_-, S' \to 0 \end{aligned} \tag{22}$$

[32] Imposing these conditions, we immediately obtain the integration constant:

$$B = P_{cm}(S_-) = P_{cm}(S_+). \tag{23}$$

[33] Therefore the solution satisfies the essential requirement that P_c is necessarily continuous across the shock. Since the relaxation term $\tau(S)$ is always positive, we can rearrange equation (21) in the limit $\varepsilon \to 0$ as:

$$\frac{dS}{d\xi} = \frac{P_{cm}(S_\pm) - P_{cm}(S)}{v\tau(S)}. \tag{24}$$

[34] This first order ODE describes the inner structure of the shock. It will be a physical solution if the saturation profile $S(\xi)$ is uniquely valued. To avoid a multiple-valued solution, $dS/d\xi$ cannot cross zero and, since the relaxation term $\tau(S)$, is positive, this implies that $P_{cm}(S) - P_{cm}(S_\pm)$ cannot cross zero. As this is an imbibition process, $S_- > S_+$, S monotonically increases with time over the jump, and therefore $dS/d\xi < 0$. This in turn implies that

$$P_{cm}(S) \geq P_{cm}(S_-) \text{ for all } S \in (S_+, S_-). \tag{25}$$

[35] This condition, together with the condition that the shock states S_- and S_+ cannot be inside the unstable region, can only be satisfied for one pair of S_- and S_+, namely the pair with S_+ at the lowest capillary pressure in the nonmonotonic P_{cm}-S curve,

$$S_+ = S_a, \tag{26}$$

and the corresponding S_- for which the capillary pressure is the same,

$$P_c(S_-) = P_c(S_a). \tag{27}$$

[36] This is shown graphically in Figure 6. Using this construction, we determine uniquely the shock states S_- and S_+. Simple integration of equation (24) provides the inner shock structure. Equations (8) and (15) provide the outer solution. This completes the construction of the traveling wave solution with nonmonotonic capillary pressure when the initial and injected states (S_∞ and $S_{-\infty}$, respectively) are outside the unstable range of increasing capillary pressure. Importantly, the take off and landing points of the jump (S_+ and S_-) are independent of the behavior at infinity, as long as these conditions span the nonmonotonic region. Therefore two qualitatively different types of solution are possible, depending on the relative values of S_- and $S_{-\infty}$ [*Witelski*, 1996]. If $S_{-\infty} > S_-$, then the entire solution is monotonically decreasing, and one such solution is shown in Figure 7.

[37] We now consider the situation where the top boundary condition $S_{-\infty}$ is in the range $S_a < S_{-\infty} < S_-$ (in particular, this encompasses the interesting case when the saturation at the top boundary is in the unstable range of increasing capillary pressure). Here again, the solution given by equation (10) is multivalued in space, and thus requires a shock. As in the solution above, the relaxation-

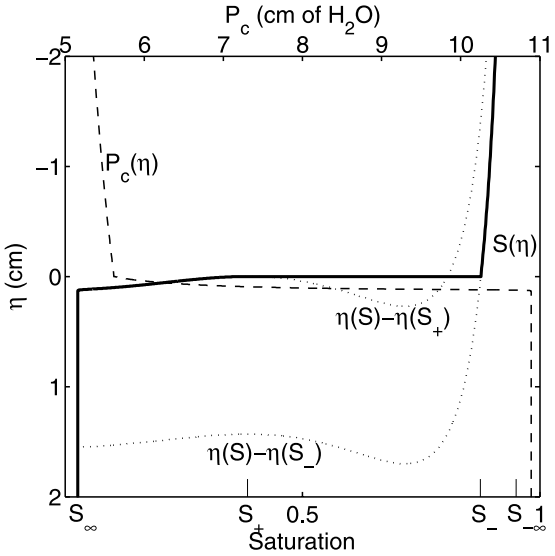

Figure 7. Complete infiltration solution ($S(\eta)$, solid line) using a nonmonotonic capillary pressure curve. The saturation shock connects the outer solutions (dotted lines) which are offset in space. Capillary pressure ($P_c(\eta)$, dashed line) is necessarily continuous in space.

type regularization term still requires that the take off and landing saturations of the shock be S_+ and S_-, respectively. After this shock the saturation then must decrease with increasing time (decreasing η) to get to $S_{-\infty}$. This last part is simply a solution of equation (8) with a drainage P_c-S curve to compute the traveling wave profile upstream of the shock (exactly the drainage solution shown by *Selker et al.* [1992]). For the solution to exist, we must assume that the drainage curve is monotone. In this case, the shock produces a saturation overshoot at the tip of the front, and the traveling wave solution is nonmonotonic. In all other manners the solution is identical to the monotonic solution described earlier. This solution construction is shown in Figures 8 and 9. These were constructed using a scanning drainage curve obtained using Scott's hysteresis model [*Scott et al.*, 1983; *Eliassi and Glass*, 2003], and the parameters and functions listed in Tables 1 and 2.

5. Second-Order Hyperbolic Correction

[38] *Eliassi and Glass* [2002, 2003] also suggested the possibility of adding a second order in time "hyperbolic" term as a means to create nonmonotonic profiles. When added to the standard Richards equation, one obtains:

$$\phi\frac{\partial S}{\partial t}+\frac{\partial}{\partial z}\left[K(S)+K(S)\frac{\partial P_c(S)}{\partial z}\right]+\frac{\partial}{\partial t}\left[T(S)\frac{\partial S}{\partial t}\right]=0. \quad (28)$$

[39] The new phenomenological coefficient $T(S)$ has units of time. The origin of this hyperbolic term stems from the observation that diffusivity equations propagate information at infinite speed, which is deemed unphysical. In the context of heat transfer, the hyperbolic correction incorporates an inertial-like effect that leads to the Cattaneo extension of Fourier's Law and results in a finite propagation speed [*Cattaneo*, 1958; *Compte and Metzler*, 1997]. Although there are no standard guidelines for the proper modeling of the phenomenological coefficient $T(S)$, it is clear that it must be a positive quantity for all values of S. For convenience, and also in the light of some physical arguments related to nonequilibrium formulations of multiphase flow [*Barenblatt*, 1971; *Barenblatt et al.*, 2003], we choose the following algebraic expression:

$$T(S)=K(S)\Gamma'(S), \quad (29)$$

where $K(S)$ is the unsaturated conductivity, and $\Gamma(S)$ is a strictly positive and monotonically increasing function (so that its derivative $\Gamma'(S)$ is also positive). Moreover, we shall consider a relaxation-type regularization, as before. Therefore the extended equation reads:

$$\phi\frac{\partial S}{\partial t}+\frac{\partial}{\partial z}\left[K(S)+K(S)\frac{dP_c(S)}{dS}\frac{\partial S}{\partial z}\right]+\frac{\partial}{\partial t}\left[K(S)\frac{\partial\Gamma(S)}{\partial t}\right]-\varepsilon\frac{\partial}{\partial z}\left[K(S)\frac{\partial}{\partial z}\left(\tau(S)\frac{\partial S}{\partial t}\right)\right]=0. \quad (30)$$

[40] We look for a traveling wave solution of the form $S(z, t) = S(\eta)$ with $\eta = z - vt$. Integrating using the same behavior at infinity as before (equation (7)), we obtain the following ODE:

$$K(S)-K(S_\infty)-v\phi(S-S_\infty)+K(S)\left(\frac{dP_c(S)}{d\eta}+v^2\frac{d\Gamma(S)}{d\eta}+\varepsilon v\frac{d}{d\eta}\left(\tau(S)\frac{dS}{d\eta}\right)\right)=0. \quad (31)$$

[41] It is straightforward to identify the effective diffusivity

$$D(S)=K(S)\left(-P_c'(S)-v^2\Gamma'(S)\right). \quad (32)$$

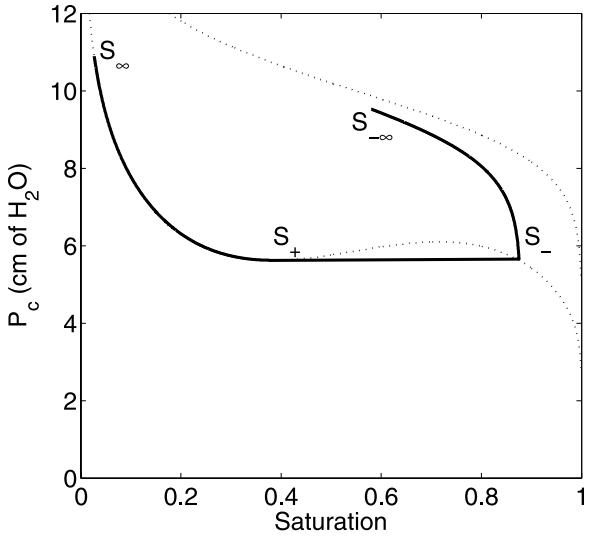

Figure 8. Path through capillary pressure–saturation space for a nonmonotonic solution. The dotted curves are the main imbibition and drainage curves. Scott's hysteresis model [*Scott et al.*, 1983] was used to generate the drainage scanning curve from S_- to $S_{-\infty}$.

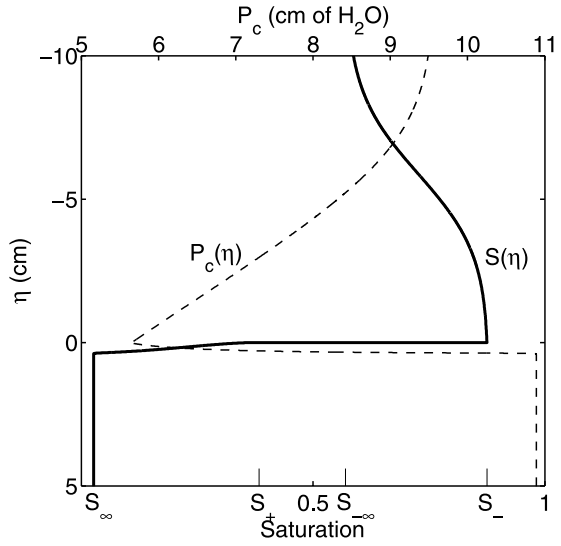

Figure 9. Complete infiltration solution when the final saturation is such that $S_a < S_{-\infty} < S_-$. This solution leads to a nonmonotonic saturation and capillary pressure profile in space.

[42] It is important to note that this effective diffusivity is only for a traveling wave solution. This is in contrast to the hypodiffusive term, which had gradients in space similar to the capillary pressure, and thus the hypodiffusive term could be completely subsumed into the capillary pressure. The inertial term has gradients in time and cannot be subsumed into the capillary pressure. If the capillary pressure is monotonic, the first term on the right hand side leads to a uniformly positive diffusivity. Negative values of the diffusivity may occur, however, if the hyperbolic contribution is sufficiently large. It is worth noting that this will depend not only on the form of the function $\Gamma(S)$, but also on the Rankine–Hugoniot velocity v, reflecting the inertial-like nature of this term.

[43] In the limit $\varepsilon \to 0$, the outer solution $\eta(S)$ is given by direct integration of the following ODE:

$$d\eta = \frac{K(S)\left(-P_c'(S) - v^2\Gamma'(S)\right)}{K(S) - K(S_\infty) - v\phi(S - S_\infty)} dS. \tag{33}$$

[44] As before, the solution will be multivalued in space if the numerator is not positive for the entire saturation range between S_∞ and $S_{-\infty}$. In that case, we must insert a shock in the traveling wave profile and use the same "shifting" principle as before. Noting the strict analogy between the integrand of equations (33) and (10), we use singular perturbation analysis and follow the same steps as in the nonmonotonic capillary pressure case, to arrive at the ODE describing (to first order) the inner structure of the shock:

$$P_c(S) + v^2\Gamma(S) + v\tau(S)\frac{dS}{d\xi} = C + O(\varepsilon). \tag{34}$$

[45] Integrating with respect to the stretched variable ξ and imposing the behavior at infinity (equation (22)), we immediately obtain the integration constant:

$$C = P_c(S_-) + v^2\Gamma(S_-) = P_c(S_+) + v^2\Gamma(S_+). \tag{35}$$

[46] The essential observation is that the traveling wave solution is no longer continuous in the capillary pressure, but in the function

$$G(S) = P_c(S) + v^2\Gamma(S), \tag{36}$$

reflecting the influence of the inertial term in the energy functional associated with the problem, as in this case there is kinetic energy (inertial term) to go with the potential energy (capillary pressure). Once again, since the relaxation term $\tau(S)$ is always positive, we can rearrange the first order ODE that describes the inner structure of the shock in the limit $\varepsilon \to 0$ as follows:

$$\frac{dS}{d\xi} = \frac{G(S_\pm) - G(S)}{v\tau(S)}. \tag{37}$$

[47] The construction of the solution, that is, the determination of the shock states S_- and S_+, is now strictly analogous to the case of nonmonotonic capillary pressure, except that now the relevant function is $G(S)$ instead of $P_c(S)$.

[48] Using a constant $\Gamma'(S) = 100$ s^2/cm, Figure 10 shows the predicted region of negative diffusivity as a function of saturation and velocity of the front for a P_c-S curve of Figure 2 and Table 1. The lower locus of points is the saturation (S_a) which corresponds to the local minimum of $G(S)$ at a particular velocity, and the upper locus is the saturation (S_b) which corresponds to the local maximum. At a particular velocity, the take-off saturation of the shock for this regularization is the local minimum ($S_+ = S_a$), and the

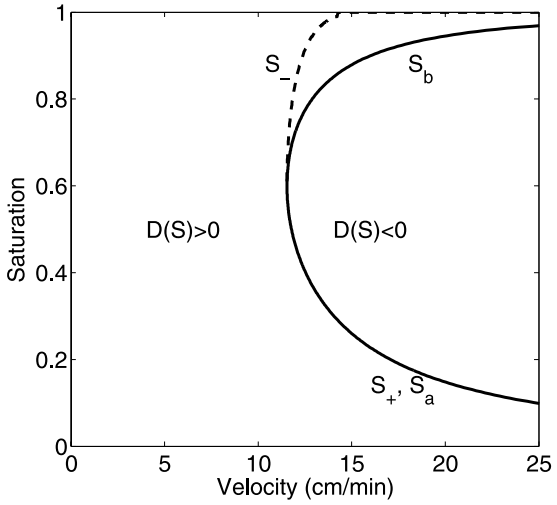

Figure 10. Region of negative diffusivity (to the right of the solid line), and landing saturation for the shock (dashed line) for the hyperbolic addition to Richards equation. We have used the constitutive curves in Table 1 and $\Gamma'(S) = 100$ s^2/cm.

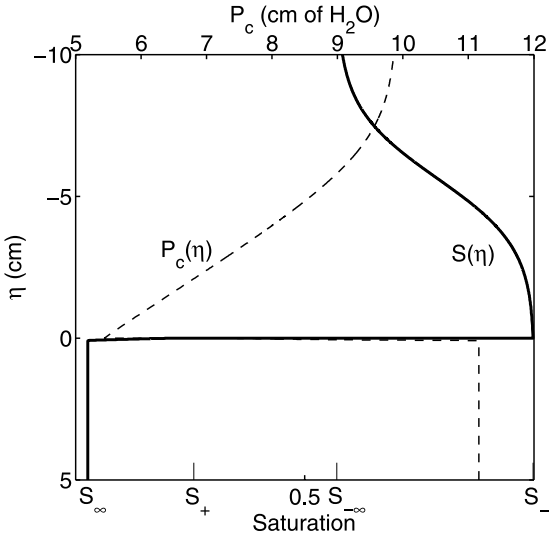

Figure 11. Complete infiltration solution for the hyperbolic (inertial) term, using the constitutive curves in Figure 2 and $\Gamma'(S) = 100\ s^2/cm$. Solution is very similar to that found for a nonmonotonic capillary pressure (Figure 9), except for this case the capillary pressure is not continuous.

dashed line gives the landing saturation (S_- obtained by $G(S_-) = G(S_a)$). In contrast to the nonmonotonic capillary pressure, the landing saturation does depend on the boundary conditions through the wave velocity. The landing saturation quickly becomes unity with increasing velocity. The choice of the magnitude of the inertial term was arbitrary; a larger inertial term will cause the negative diffusivity region to lower velocities. Also a different functional form for $\Gamma(S)$ will alter the shape of the negative diffusivity region slightly.

[49] Figure 11 shows the full spatial solution with the same boundary conditions as used for the nonmonotonic case and a constant $\Gamma'(S) = 100\ s^2/cm$. As with the other possible additional terms, here we have assumed that the inertial term is zero on drainage. The overall solution is very similar to that predicted for a nonmonotonic P_c-S curve, with the differences being that the capillary pressure is not continuous and slightly different take-off and landing saturations.

6. Discussion

[50] As there are similarities in the two solutions presented, we first discuss the solution obtained with the nonmonotonic P_c-S curve followed by the solution with the inertial term. The features of the mathematical solution with a nonmonotonic P_c-S curve can be summarized in the following bulleted points

[51] 1. Assuming the initial saturation is below the nonmonotonic region of the P_c-S curve ($S_{+\infty} < S_a$), the profile will be nonmonotonic if the final saturation is in the range $S_a < S_{-\infty} < S_-$. Thus the profile will be nonmonotonic for an applied flux q within the range of $K(S_a) < q < K(S_-)$.

[52] 2. The landing (or tip) saturation is independent of the flux, and is given by S_-.

[53] 3. The nonmonotonic saturation profiles show a spatially abrupt jump from the initial condition to the landing saturation.

[54] The inertial term solution produces slightly different results:

[55] 1. The profile will be monotonic until the infiltration velocity is high enough such that there will be a saturation region of negative diffusivity. Above this velocity, the profile will be nonmonotonic if the upstream condition has a negative diffusivity.

[56] 2. The landing (or tip) saturation depends on the flux, but rapidly becomes unity with increasing flux.

[57] 3. The nonmonotonic saturation profiles show a spatially abrupt jump from the initial condition to the landing saturation.

[58] We now compare these two solutions to the experiments in order to see which features are replicated. As mentioned previously, the physics behind the initial wetting front is well described by traditional equations, and since all of the models use the traditional physics for the drainage curve, they all fit equally well for this portion of the observed nonmonotonicity. Thus the features we will be comparing are the features that have to do with the behavior at the initial wetting front. In particular these are the initial wetting front saturation (tip saturation) as a function of flux and porous medium, and the physical length of the initial wetting front.

[59] First, we discuss the saturation versus space and the length of the initial wetting front as seen in Figures 1, 9, and 11. Experimentally, we observe that the initial wetting front into these porous media is extremely localized in space, and can be considered on the order of the grain size. Both of the continuum extensions discussed here predict a discontinuous saturation when the profile is nonmonotonic. Thus both of the extensions solved for in this paper fare very well on

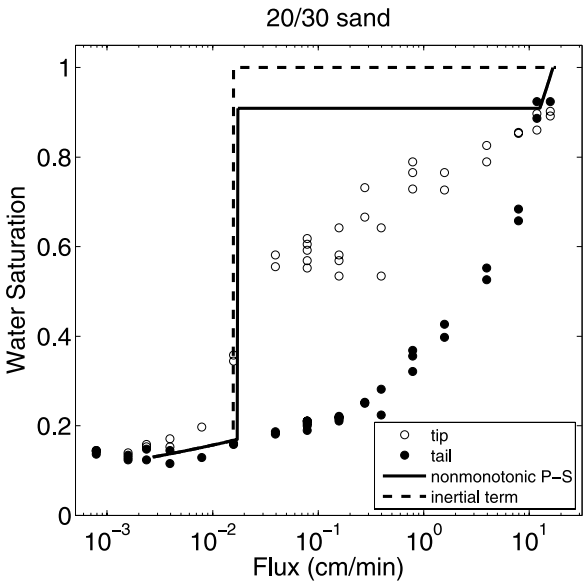

Figure 12. Best fits of the experimentally measured tip saturation using the nonmonotonic P_c-S curve (solid line) and the inertial term (dashed line). For this case, both models predict an abrupt transition between monotonic and nonmonotonic solutions. The coefficients obtained from fitting this transition flux to the 20/30 sand are then used for the other sized sands without further modification.

Table 3. Parameters That Obtained the Best Fit for the 20/30 Sand[a]

Name	Symbol	Functional Form
Unsaturated conductivity	$K(S)$	$K_S \begin{cases} S^3 & S \geq S_p \\ S^7/S_p^4 & S \leq S_p \end{cases}$
Hypo-diffusive term	$\Lambda(S)$	$\frac{1}{\alpha}(1 - S_e)^2$
Hypo-diffusive magnitude	N_{HD}	1.05
Inertial magnitude	Γ'	4×10^5 s^2/cm

[a]A slightly different functional form was used for the conductivity and hypo-diffusive term. The measured unsaturated conductivity using the flux and the measured saturation $S_{-\infty}$ (final or tail saturation) was fit well by a piecewise power law function (with a break saturation of S_p). The hypo-diffusive term and magnitude and the inertial magnitude were chosen to fit the overshoot for the 20/30 sand.

this point. This is in contrast to the relaxation extension which predicts an initial wetting front of several centimeters [*DiCarlo*, 2005].

[60] Second, we compare the experimentally measured tip saturation to the two model extensions. All of the extensions have a fitting parameter, so instead of trying to fit the tip saturation at one particular flux, we attempt to find the best fitting parameter for the range of fluxes. Figure 12 shows the tip saturation measured with light transmission (open circles), and the two best fits for the nonmonotonic P_c-S curve (solid line) and the inertial term (dashed line). Here the porous medium is 20/30 sand (median grain size 0.71 mm, see Table 2). As can be seen, the extensions are easily capable of matching the transition flux between monotonic and non-monotonic profiles (experimentally measured for this medium to be at a flux of 0.02 cm/min).

[61] The fits were obtained as follows. For the requisite constitutive curves, we use a van Genuchten P_c-S curve which was fit to imbibition data obtained in capillary rise experiments. The measured unsaturated conductivity using the applied flux and the measured saturation $S_{-\infty}$ (final or tail saturation) was fit well by a piecewise power law function. We use these curves as the basis for all three sands and the parameters are summarized in Tables 2 and 3.

[62] To create the nonmonotonic P_c-S curve we follow the method of Eliassi and Glass and add an additional term into the capillary pressure (equation (13)), with the best fit function and parameters given in Table 3. For the inertial term fit shown in Figure 12, we use a constant inertial term of $\Gamma'(S) = 4 \times 10^5$ s^2/cm (Table 3). As can be seen, both extensions show a discontinuous jump in the tip saturation once the threshold flux is reached. Above this flux, the tip saturation is independent of flux, until very high fluxes where the profile becomes monotonic again for the nonmonotonic P_c-S curve. While the nonmonotonic P_c-S curve requires that the tip saturation be independent of flux, one can choose a different functional form for the inertial term such that the tip saturation has a slight dependence on flux. This tip dependence is only seen for fluxes within 50% of the transition flux, and thus for simplicity, we choose a constant inertial term.

[63] There are some caveats when comparing the solutions to the experimental data. First, experimental data suggests not a single transition flux, but a wider transition region of between 0.01 and 0.04 cm/min. In actuality there is only one measured flux where the tip shows an intermediate behavior, so the actual width of the transition is not clear from the data. Also any experiments will show broader transitions just due to natural variations in the media or the environmental conditions. Thus the sharp transition flux predicted by these two extensions (and the relaxation extension) is not in disagreement with the experimental data. Secondly, the experimental measurements show a tip saturation that increases slowly with flux even when the nonmonotonic profiles are observed (i.e., for fluxes between 0.1 and 10 cm/min). As mentioned in a previous paper [*DiCarlo*, 2006], this tip saturation dependence with flux is not definitive, and is currently being investigated further using tomographic measurements. Solutions with a relaxation term [*DiCarlo*, 2005], and dynamic network modeling predictions [*DiCarlo*, 2006] of the tip saturation also predict a fully saturated tip.

[64] One possibility that we explore here is to use the parameters obtained from the 20/30 sand and to see how well the tip saturations and transition flux is predicted for other porous media. To do this we use the exact extensions that were obtained for the fit to the 20/30 sand, and use these with the soil parameters for the other porous media. Figure 13 shows the comparison with the extensions for the finer 30/40 sand. Experimentally, this sand shows a higher transition flux, and a more saturated tip after the transition (which is probably the result of the walls of the column). The nonmonotonic P_c-S curve actually predicts a lower transition flux than in 20/30 sand, and the inertial term predicts a slightly higher transition flux, but only 10% higher, quite a bit less than actually observed.

[65] Figure 14 shows the comparison with the extensions for the coarser 12/20 sand. Experimentally, this sand shows a lower transition flux. The nonmonotonic P_c-S curve actually predicts a higher transition flux than in 20/30 sand,

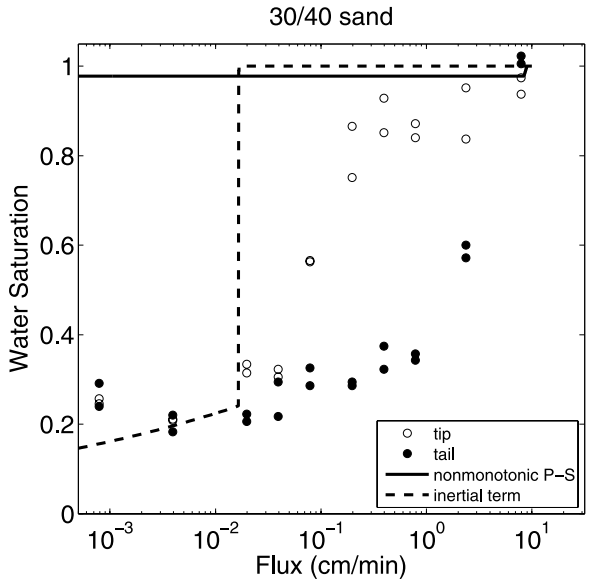

Figure 13. Experimentally measured tip saturation for finer 30/40 sand and predictions from the nonmonotonic P_c-S curve (solid line) and the inertial term (dashed line) where these predictions are from the coefficients determined from the 20/30 sand.

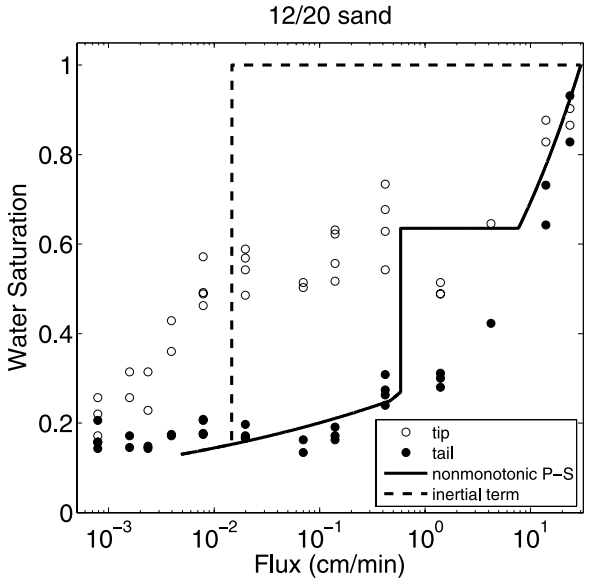

Figure 14. Experimentally measured tip saturation for coarser 12/20 sand and predictions from the nonmonotonic P_c-S curve (solid line) and the inertial term (dashed line) where these predictions are from the coefficients determined from the 20/30 sand.

and the inertial term predicts a slightly lower transition flux, but only 10% lower, quite a bit less than actually observed.

[66] Although these fits are poor, they are highly dependent on the P_c-S imbibition curve which is very difficult (if not impossible) to measure accurately for these sandy porous media, and the specifics of the functional fit. Also, the same additional terms were used for each porous medium, as any particular data set can be fit by varying the magnitudes of the additional term. Basically, the comparison to the experimental data shows that fitting one data set does not allow any predictive capabilities for another data set. This was also the case for fitting using only the relaxation term [*DiCarlo*, 2005].

[67] Comparing the nonmonotonic P_c-S curve, and the inertial term, the inertial term makes slightly more physical sense. This is because the inertial term will be negligible during slow capillary rise experiments, and thus it can match the gradual profiles seen in these types of experiments as well as the sharp profiles seen in dynamic infiltration experiments. Also, the inertial term is a natural extension, as water does, of course, have inertia. The Navier-Stokes equation gives an inertia value of roughly $\Gamma'(S) = 1/g = 10^{-3}$ s^2/cm. However, this value is over eight orders of magnitude less than what is needed to roughly match the observed transition velocity ($\Gamma' = 4 \times 10^5$ s^2/cm). This is not unexpected, as it is well known that porous media flows are viscously dominated. Thus the ''inertia'' in the inertial term has to come from some other physical effect besides real inertia to produce the observed overshoot.

[68] Both of these solutions create a nonmonotonic saturation profile using a continuum description of the porous medium. Arguments have been made that the actual physics creating the nonmonotonic profiles is a wetting front that is sharp at the pore-scale [*Eliassi and Glass*, 2001, 2002; *DiCarlo*, 2004; *Shiozawa and Fujimaki*, 2004; *Annaka and Hanayama*, 2005; *DiCarlo*, 2005; *DiCarlo*, 2006]. Thus discrete pore filling mechanisms play a large role, and the physics cannot be accurately described at the continuum scale. Still, as all large scale models are based on continuum formulations, the addition of a continuum term that reproduces much of the observed behavior may be an effective mathematical model. All three possible extensions postulated by Eliassi and Glass (nonmonotonic P_c-S, inertial term, finite relaxation term) produce nonmonotonic profiles. In terms of continuum modeling, it is still unclear as to which model is more appropriate for applications. Indeed, it may be that different extensions are appropriate for different situations. Using multiple additional terms (e.g., inertial and relaxation) will most likely produce better fits to the data, but of course, the draw back is one more additional fitting parameter.

[69] The saturation profiles of *Eliassi and Glass* [2003] using a nonmonotonic P_c-S curve do not follow the construction outlined in this paper, as the take off point of their shock is not from the local minimum of the P_c-S curve. This can be seen for the numerical simulation for the medium with $n = 11$ in Figures 9 and 11b of their paper [*Eliassi and Glass*, 2003]. Their numerical simulations are obtained without a regularization term. Thus, theoretically, all jumps satisfying that saturation states across the shock have the same capillary pressure are equally valid. Any numerical simulation implicitly produces higher order terms through the space and time discretization, which then act as regularization terms, even if they decrease as the grid is refined. It is not surprising that the solutions do not match up as the regularization is likely to be different. The analytic solution construction above can be extended to different regularization terms (e.g., fourth-order in space, characteristic of the implicit regularization from numerical simulation), if one so desires [*Witelski*, 1995].

[70] In summary, we have shown how to obtain traveling wave solutions to infiltrations into porous media, where the flow equations are extended with either a hypodiffusive (nonmonotonic P_c) or hyperbolic (inertial) term. The solutions exhibit nonmonotonic saturation profiles when the diffusivity is negative for a range of saturations. The physical accuracy of these extensions is debatable. As evidenced by comparison of Figure 1 with Figures 9 and 11, the solutions match certain features of the observed infiltrations (e.g., transition flux, sharp wetting front), but match poorly other features (e.g., landing saturation, capillary rise, very large inertial term). Although either extension can be used to adequately fit the observed overshoot for a particular porous medium, the matched parameters are not invariant among porous media.

[71] **Acknowledgments.** The authors thank Martin Blunt and Hung Pham for helpful discussions, and Jean-Yves Parlange, and three anonymous reviewers for helpful reviews.

References

Annaka, T., and S. Hanayama (2005), Dynamic water-entry pressure for initially dry glass beads and sea sand, *Vadose Zone J.*, *4*, 127–133.

Barenblatt, G. I. (1971), Filtration of two nonmixing fluids in a homogeneous porous medium. Soviet Academy Izvestia, *Mechanics of Gas and Fluids*, *5*, 857.

Barenblatt, G. I., T. W. Patzek, and D. B. Silin (2003), The mathematical model of nonequilibrium effects in water-oil displacements, *SPE J.*, *8*, 409–416.

Bear, J. (1972), *Dynamics of Fluids in Porous Media*, American Elsevier, New York.

Cattaneo, C. (1958), A form of heat conduction equation which eliminates the paradox of instantaneous propagation, *Comp. Rend.*, *247*, 431–433.

Compte, A., and R. Metzler (1997), The generalized Cattaneo equation for the description of anomalous transport processes, *J. Phys. A Math. Gen.*, *30*, 7277–7289.

Cuesta, C., and J. Hulshof (2003), A model problem for groundwater flow with dynamic capillary pressure: Stability of traveling waves, *Nonlinear Analysis*, *52*, 1199–1218.

Cuesta, C., C. J. van Duijn, and J. Hulshof (2000), Infiltration in porous media with dynamic capillary pressure: Traveling waves, *Eur. J. Appl. Math.*, *11*, 381–397.

DiCarlo, D. A. (2004), Experimental measurements of saturation overshoot on infiltration, *Water Resour. Res.*, *40*, W04215, doi:10.1029/2003WR002670.

DiCarlo, D. A. (2005), Modeling observed saturation overshoot with continuum additions to standard unsaturated theory, *Adv. Water Resour.*, *28*, 1021–1027.

DiCarlo, D. A. (2006), Quantitative network model predictions of saturation behind infiltration fronts and comparison to experiments, *Water Resour. Res.*, *42*, W07408, doi:10.1029/2005WR004750.

Dullien, F. A. L. (1992), *Porous Media: Fluid Transport and Pore Structure*, 2nd edition, Academic, Inc., San Diego, CA.

Egorov, A. G., R. Z. Dautov, J. L. Nieber, and A. Y. Sheshukov (2003), Stability analysis of gravity-driven infiltrating flow, *Water Resour. Res.*, *39*(9), 1266, doi:10.1029/2002WR001886.

Eliassi, M., and R. J. Glass (2001), On the continuum-scale modeling of gravity-driven fingers in unsaturated porous media: The inadequacy of the Richards equation with standard monotonic constitutive relations and hysteretic equations of state, *Water Resour. Res.*, *37*, 2019–2035.

Eliassi, M., and R. J. Glass (2002), On the porous-continuum modeling of gravity-driven fingers in unsaturated materials: Extension of standard theory with a hold-back-pile-up effect, *Water Resour. Res.*, *38*(11), 1234, doi:10.1029/2001WR001131.

Eliassi, M., and R. J. Glass (2003), On the porous continuum-scale modeling of gravity-driven fingers in unsaturated materials: Numerical solution of a hypodiffusive governing equation that incorporates a hold-back-pile-up effect, *Water Resour. Res.*, *39*(6), 1167, doi:10.1029/2002WR001535.

Geiger, S. L., and D. S. Durnford (2000), Infiltration in homogeneous sands and a mechanistic model of unstable flow, *Soil Sci. Soc. Am. J.*, *64*, 460–469.

Gray, W. G., and S. M. Hassanizadeh (1991), Unsaturated flow theory including interfacial phenomena, *Water Resour. Res.*, *27*, 1855–1863.

Hassanizadeh, S. M., and W. G. Gray (1990), Mechanics and thermodynamics of multiphase flow in porous media including interphase boundaries, *Adv. Water Resour.*, *13*, 169–186.

Hassanizadeh, S. M., M. A. Celia, and H. K. Dahle (2002), Dynamic effect in the capillary pressure-saturation relationship and its impacts on unsaturated flow, *Vadose Zone J.*, *1*, 38–57.

Hillel, D. (1980), *Applications of Soil Physics*, Academic, Inc., San Diego, CA.

Hollig, K. (1983), Existence of infinitely many solutions for a forward backward heat equation, *Trans. AMS*, *1*, 299–316.

Nieber, J. L., R. Z. Dautov, A. G. Egorov, and A. Y. Sheshukov (2005), Dynamic capillary pressure mechanism for instability in gravity-driven flows: Review and extension to very dry conditions, *Transp. Porous Media*, *58*, 147–172.

Scott, P. S., G. J. Farquhar, and N. Kouwen (1983), Hysteretic effects on net infiltration. Pages 163–170 in *Advances in Infiltration*, Am. Soc. of Agric. Eng., St. Joseph, Mich.

Selker, J., J.-Y. Parlange, and T. Steenhuis (1992), Fingered flow in two dimensions: 2. Predicting finger moisture profile, *Water Resour. Res.*, *28*, 2523–2528.

Shiozawa, S., and H. Fujimaki (2004), Unexpected water content profiles under flux-limited one-dimensional downward infiltration in initially dry granular media, *Water Resour. Res.*, *40*, W07404, doi:10.1029/2003WR002197.

Stonestrom, D. A., and K. C. Akstin (1994), Nonmonotonic matric pressure histories during constant flux infiltration into homogeneous profiles, *Water Resour. Res.*, *30*, 81–91.

van Duijn, C. J., L. A. Peletier, and I. S. Pop (2007), A new class of entropy solutions of the Buckley–Leverett equation, *SIAM J. Mathematical Analysis*, *39*, 507–536.

Witelski, T. P. (1995), Shocks in nonlinear diffusion, *Appl. Math. Lett.*, *8*, 27–32.

Witelski, T. P. (1996), The structure of internal layers for unstable nonlinear diffusion equations, *Stud. Appl. Math.*, *97*, 277–300.

D. A. DiCarlo, Petroleum and Geosystems Engineering, The University of Texas at Austin, Austin, TX, USA. (dicarlo@mail.utexas.edu)

R. Juanes, Department of Civil and Environmental Engineering, Massachusetts Institute of Technology, Cambridge, MA, USA. (juanes@mit.edu)

T. LaForce, Department of Earth Science and Engineering, Imperial College London, London, UK. (t.laforce@imperial.ac.uk)

T. P. Witelski, Department of Mathematics, Duke University, Durham, NC, USA. (witelski@math.duke.edu)